Self-Ordering Behavior of Anodic Porous Alumina via Selenic Acid Anodizing

Tatsuya Kikuchi*, Osamu Nishinaga, Shungo Natsui, and Ryosuke O. Suzuki
Faculty of Engineering, Hokkaido University
N13-W8, Kita-ku, Sapporo, Hokkaido, 060-8628, Japan

*Corresponding author: Tatsuya Kikuchi
TEL: +81-11-706-6340
FAX: +81-11-706-6342
E-mail: kiku@eng.hokudai.ac.jp

Abstract

The self-ordering behavior of anodic porous alumina that was formed by anodizing in selenic acid electrolyte (H_2SeO_4) at various concentrations and voltages was investigated with SEM and AFM imaging. A high purity aluminum foil was anodized in 0.1-3.0 M selenic acid solutions at 273 K and at constant cell voltages in the range of 37 to 51 V. The regularity of the cell arrangement increased with increasing anodizing voltage and selenic acid concentration under conditions of steady oxide growth without burning. Anodizing at 42-46 V in 3.0 M selenic acid produced highly ordered porous alumina. By selective dissolution of the anodic porous alumina, highly ordered convex nanostructures of aluminum with diameters of 20 nm and heights of 40 nm were exposed at the apexes of each hexagonal dimple array. Highly ordered anodic porous alumina with a cell size of 102 nm from top to bottom can be fabricated by a two-step selenic acid anodizing process, that includes the first anodizing step, the selective oxide dissolution, and the second anodizing step.

Key words: Aluminum; Anodizing; Anodic Porous Alumina; Selenic Acid

1. Introduction

Barrier anodic oxide films and porous anodic oxide films on aluminum have been widely investigated by many researchers in the fields of surface finishing [1-3], electrolytic capacitor application [4-6], and micro- and nano-structure fabrication [7-9]. Recently, highly ordered anodic porous alumina with a cell size on the scale of 10-100 nm has been studied for potential use in various ordered-nanostructure applications [10-21]. Anodic porous alumina is typically fabricated on an aluminum substrate using electrochemical anodizing (or anodization) [22-26]. In several acidic electrolyte solutions, the porous alumina fabricated by anodizing is self-ordered when prepared at the appropriate electrochemical conditions, including appropriate concentrations, temperatures, and voltages (or electrochemical potentials) [27-30].

Sulfuric (H_2SO_4) [31], oxalic ($(COOH)_2$) [7, 32], and phosphoric (H_3PO_4) [33] acids are the three major electrolytes used for anodic porous alumina fabrication; many researchers have investigated the highly ordered anodic porous alumina formed by anodizing in these three electrolytes [34-36]. Malonic (HOOC-CH_2-COOH) [28, 37-39] and tartaric ($HOOC(CHOH)_2COOH$) [28, 40] acids are also known self-ordering electrolytes, as reported previously. However, malonic and tartaric acids have seldom been used for nanostructure fabrication because they do not perform as well with regards to self-ordering as the three major electrolytes. Chromic (H_2CrO_4) [41-43], formic (HCOOH) [44], malic (HOOC-CH(OH)-CH_2-COOH) [27, 45, 46], citric (HOOC-CH_2-C(OH)(COOH)-CH_2-COOH) [27, 47, 48], glycolic (CH_2OH-COOH) [27], squaric (3,4-dihydroxy-3-cyclobutene-1,2-dione) [49], tartronic (HOOC-CH(OH)-COOH) [50], and acetylenedicarboxylic (HOOC-C≡C-COOH) [51] acids have also been reported as electrolytes used to fabricate porous alumina that has characteristic nanostructure morphologies.

In addition to these acidic electrolytes, alkaline and neutral solutions used for porous alumina fabrication were reported by several research groups. Takahashi et al. reported that a porous anodic oxide film could be formed by anodizing in an $H_3BO_3/Na_2B_4O_7$ neutral borate solution at a high temperature [52]. Baron-Wiechec et al. investigated aluminum anodizing in a borax ($Na_2B_4O_7$) solution at 333 K and successfully obtained porous alumina [53]. Noguchi et al. investigated the anodizing behavior of aluminum in propylenediamine and choline alkaline solutions containing ammonium fluoride, ammonium tartrate, ammonium carbonate, and ammonium tetraborate, and obtained anodic porous alumina with nanopores that were 10-150 nm in diameter [54]. However, it is difficult to form a highly ordered porous alumina by anodizing in these neutral and alkaline solutions. Therefore, acidic solutions, especially the three major electrolytes (sulfuric, oxalic, and sulfuric acids), are typically used for anodic porous alumina fabrication.

In 2013, we first reported a new self-ordered anodic porous alumina fabrication method that used selenic acid (H_2SeO_4) anodizing [55]. Selenic acid is easily soluble in water, and is a strong diacid with dissociation constants of $pKa_1 = -3.0$ and $pKa_2 = 1.7$,

which are the same as those of sulfuric acid. Selenic acid solution dissolves silver, gold, and palladium metals. Standard electrode potentials related to selenic acid are as follows:

$$SeO_4^{2-} + 4H^+ + 2e^- = H_2SeO_3 + H_2O,\ E° = 1.151\ V \quad (1)$$

$$H_2SeO_3 + 4H^+ + 4e^- = Se + 3H_2O,\ E° = 0.739\ V \quad (2)$$

In our previous study, self-ordered porous alumina was rapidly produced by 0.3 M selenic acid anodizing using a simple electrochemical setup, and the porous alumina obtained had nanopores on the scale of 10 nm at the center of each cell. The concentration of the selenic acid solution was fixed at the typical anodizing concentration of 0.3 M. Stirring vigorously at low temperature (273 K) during selenic acid anodizing was required to achieve self-ordering. The anodic porous alumina produced by anodizing in the solution was only self-ordered at 48 V. However, the details of the self-ordering behavior of the anodic porous alumina during selenic acid anodizing at different solution concentrations and voltages had not been studied so far, and further investigation will be required for highly ordered nanostructure applications.

In the present investigation, we report on the self-ordering behavior of anodic porous alumina fabricated by anodizing at various voltages in various concentrations of selenic acid solution. The anodic porous alumina fabricated by selenic acid anodizing was examined in details by scanning electron microscopy (SEM) and atomic force microscopy (AFM). We found that the regularity of the anodic porous alumina formed by selenic acid anodizing was greatly improved with increasing anodizing voltage and electrolyte concentration. This observed improvement expands the range of voltages that can be used for the fabrication of self-ordered anodic porous alumina as well as the range of ideal hexagonal cell sizes, and it therefore expands the applicability of anodic porous alumina.

2. Experimental

2.1 Pretreatment and selenic acid anodizing

Aluminum foils (99.99 wt%, 110 μm thick, Showa Aluminum Co., Japan, impurities: Fe 10 ppm, Si 9 ppm, and Cu 57 ppm) were used as the anodizing specimens. The specimens were cut into 20 mm x 20 mm pieces with a handle and then ultrasonically degreased in an ethanol solution for 10 min. After degreasing, the specimens were electropolished in a 13.6 M CH_3COOH/2.56 M $HClO_4$ mixed solution at 280 K at a constant voltage of 28 V for 60 s. A large aluminum plate (99.99 wt%) was used as the counter electrode, and the solution was slowly stirred with a magnetic stirrer during electropolishing. The electropolished specimens were then washed with distilled water and dried in a desiccator.

Figure 1 shows a schematic model of the selenic acid anodizing setup. An extremely simple two-electrode electrochemical cell with a low temperature water bath was used in the anodizing process. For the fabrication of anodic porous alumina, selenic acid (80.0 wt%, Kanto Chemical Co., Japan) was used as the anodizing electrolyte. The

electropolished specimens were immersed in H_2SeO_4 solutions with concentrations in the range of 0.1 to 3.0 M at 273K and were placed parallel to and 15 mm from a glassy carbon cathode (1 mm thick, Tokai Carbon Co., Japan). Using the anodizing electrolyte at the low temperature of 273 K is an effective way to fabricate a self-ordered anodic oxide without burning [55]. After placement in the solutions, the specimens anodized for 180 min at a constant voltage in the range of 37 to 51 V (direct current power supply PWR400H, Kikusui, Japan). During anodizing, the solutions were vigorously stirred with a magnetic stirrer and the current densities were recorded using a digital multimeter (DMM4040, Tektronix) connected to a computer. After anodizing, the specimens were quickly removed from the solution, washed with distilled water, and dried in a desiccator.

2.2 Second selenic acid anodizing

The aluminum specimen that was anodized at 46 V for 180 min in the 3.0 M H_2SeO_4 solution, as described above, was immersed in a 0.20 M CrO_3/0.51 M H_3PO_4 solution at 353 K to dissolve selectively the anodic porous alumina. This specimen was then anodized again at a constant voltage of 46 V for 3 min in a 3.0 M H_2SeO_4 solution (two-step anodizing). Thus, the two-step anodizing process includes the first anodizing, the oxide dissolution, and the second anodizing. To widen the pores in the anodic porous alumina, the specimen was immersed in a 0.86 M H_3PO_4 solution at 293 K for 10 min.

2.3 Characterization of the anodic porous alumina

The surface morphologies of the specimens were examined after the first anodizing, after the oxide dissolution, and after the second anodizing using an SEM (JSM-6500F and JIB-4600F/HKD, JEOL, Japan, and Miniscope TM-1000, Hitachi, Japan) and an AFM (Nanocute, Hitachi, Japan, with the internal sensor type of cantilever). For the SEM observations of the anodic porous alumina, a platinum electro-conductive layer was sputter-coated on the specimens using a sputter coater (MSP-1S, Vacuum Device Co., Japan). To examine the vertical cross sections, two treated specimens were prepared: a) one group of specimens was mechanically cut. b) the other group of specimens was embedded in an epoxy resin, polished mechanically, and then immersed in a 0.25 M $K_3[Fe(CN)_6]$/4.17 M NaOH solution at room temperature to clearly observe the anodic oxide.

3. Results and discussion

Figure 2a shows the changes in the current density with anodizing time at several voltages in the 0.1 M H_2SeO_4 solution at 273 K. At 37 V, the current density increased rapidly to over 15 A m^{-2} and then decreased to 0.6 A m^{-2} during the initial 4 min. After this initial stage, the current density gradually increased to 1.8 A m^{-2} and then held a steady value of 1.8 A m^{-2} from 40 to 180 min. The current-time transients show changes

that are typical for porous alumina. The formation behavior is explained as follows: The rapid increase and decrease of the current density at the beginning of the anodizing process correspond to a period of barrier layer formation. A thin, compact barrier layer with a withstand voltage of 37 V was rapidly formed on the aluminum substrate by constant voltage anodizing according to the following equation:

$$2Al + 3H_2O = Al_2O_3 + 6H^- + 6e^- \quad (3)$$

After the barrier oxide formation, the current then gradually decreased with increasing anodizing time because of the repairing of defects in the barrier oxide. The gradual increase in current density and its subsequent steady value correspond to the formation of pores in the barrier oxide and the steady growth of the porous layer, respectively. The voltages of 42 V and 50 V show that the plateau current density for the formation of porous alumina increased with increasing anodizing voltage. This is due to the rapid growth of the anodic porous alumina at high anodizing voltages. At 51 V, the current density increased rapidly to over 300 A m^{-2} in the initial period, and intense oxygen gas production from the aluminum specimen was observed during anodizing. This "burning phenomenon" caused by the electric current during anodizing was previously reported at ultra-high current densities in many acidic electrolytes [28, 29, 56-59].

The current density changes with anodizing time in H_2SeO_4 solutions at a higher concentration (1.0 M, 273 K) are shown in Fig. 2b. The initial transition periods, during which the barrier layer forms and the pore opening stage of the porous alumina formation occurs, were shortened to 10 min at voltages in the range of 37 to 47 V, and each plateau current density was considerably larger than that at the same anodizing voltage in the 0.1 M H_2SeO_4 solution. These effects occurred because of the rapid growth of the anodic porous alumina caused by the high concentration of the electrolyte. In addition, the critical voltage of burning decreased to 48 V in the 1.0 M H_2SeO_4 solution. This is due to the impediment to joule heat radiation from the aluminum specimen during anodizing at a high oxide growth rate. The current density effects including the rapid initial transition, the large plateau current density, and the decrease in burning voltage are even more pronounced in the 3.0 M H_2SeO_4 solution (Fig. 2c). The current density for porous alumina at 46 V gradually decreased with anodizing time, in contrast with the current densities at the other voltages. This may be because this voltage condition is the critical state between "steady state oxide growth" and "burning". Selenic acid anodizing produced a colorless, transparent anodic oxide film at all anodizing conditions that did not in burning (Fig. 3a). The mean thickness of the transparent anodic porous alumina was determined to be approximately 17 μm from the SEM observation. During selenic acid anodizing, reddish selenium was deposited on the glassy carbon cathode because of the reduction of selenate ions with hydrogen gas evolution (equations (1) and (2)).

Figure 4 shows low magnification SEM images of a typical surface of the anodized specimen a) at 46 V in a 3.0 M H_2SeO_4 solution (which exhibits porous layer growth) and b) at 51 V in a 0.1 M H_2SeO_4 solution (which exhibits burning); the current density

changes for these surfaces are shown in Figs. 2a and 2c. Figure 4a shows that the anodic oxide film, which appears as a dark gray region, was uniformly formed on the whole aluminum surface after anodizing at 46 V for 180 min in a 3.0 M H_2SeO_4 solution and that there were no imperfection on the anodic oxide film. In contrast, several cracks that are a few hundred μm in length are observed on the uneven anodic oxide film that formed during the burning phenomenon at 51 V in a 0.1 M H_2SeO_4 solution. These cracks are caused by the high current density resulting from the application of a high electric field. Oxygen gas evolution occurs at these cracks during anodizing as described previously. The formation of an anodic oxide with many imperfections has been previously reported for anodizing at a high electric field in other electrolytes such as sulfuric, phosphoric, and various carboxylic acids [28, 29, 56-59]. To avoid the formation of the uneven anodic oxide film caused by burning, the self-ordering behavior of anodic porous alumina should be examined by anodizing below the burning voltage.

When anodic porous alumina grows on aluminum during constant voltage anodizing, nanoscale pores are created in a disorderly fashion during the initial stage of anodizing. At the appropriate anodizing conditions, the nanopores gradually become ordered at the interface between the oxide and aluminum substrate [28]. Therefore, studying the oxide-aluminum interface is important to understanding the self-ordering behavior of the anodic porous alumina. The anodized specimens prepared by selenic acid anodizing at various voltages and selenic acid concentrations were immersed in a CrO_3/H_3PO_4 solution to dissolve the anodic oxide selectively, and the exposed aluminum substrates (which correspond to the bottoms of the anodic porous alumina specimens) were examined by SEM observations. Figure 5 shows SEM images of the typical aluminum substrate after anodizing at voltages in the range of 37 to 50 V in 0.1-3.0 M H_2SeO_4 solutions for 180 min. In the 0.1 M H_2SeO_4 solution (the left column in Fig. 5), disordered dimple arrays were distributed on the aluminum substrate at all anodizing voltages: 37, 42, and 50 V. A large number of dimple junctions with four and five points were observed on the surface due to the incomplete self-ordering of the anodic porous alumina. The regularity of the dimple arrangement gradually increased with increasing anodizing voltage. However, the nanostructures obtained by these anodizing conditions cannot be described as well-ordered. The average cell size (which is the same as the dimple diameter and the interpore distance) also increased with increasing anodizing voltage.

As the concentration of H_2SeO_4 increases from 0.1 M to 1.0 M (the middle column in Fig. 5), it is clear that the regularity of the dimple arrangement improved at each anodizing voltage. Within the results for the 1.0 M in H_2SeO_4 solution, the regularity improved with increasing anodizing voltage. An ideal cell arrangement (which consists of an ordered hexagonal structure) that contains more than 50 cells is observed at 42 V and 47 V. The regularity of the cell arrangement was further improved by using a 3.0 M H_2SeO_4 solution (the right column in Fig. 5). In this solution, ideal cell arrangements with more than 100 cells were formed at 42 V and 46 V. Note that highly ordered

anodic porous alumina can be obtained at 42-46 V in this solution. With SEM observations, the cell size of the anodic porous alumina was determined to be 102 nm at 46 V. These SEM observations also show that the regularity of the anodic porous alumina was strongly affected by the selenic acid concentration and that highly ordered anodic porous alumina can be fabricated by anodizing in high concentrations of selenic acid electrolyte.

The relation between the cell size and the anodizing voltage in selenic acid and other self-ordering electrolytes is now discussed below. The effects of the anodizing voltage, V, on the corresponding cell size, D, in different H_2SeO_4 concentrations were shown in Fig. 6. The mean cell size increased linearly with anodizing voltage in 3.0 M and 1.0 M selenic acid solutions. However, there is no linear relationship between these two parameters in 0.1 M selenic acid solution. The linear relation between the anodizing voltage and the cell size at the appropriate self-ordering condition has been reported by several research groups [28, 30], and it is described as follows:

$$D = 2.5\ V\ [nm] \quad (4)$$

The linear relation obtained at our self-ordering condition was consistent with those previously reported for other anodizing electrolytes, such as sulfuric, oxalic, and phosphoric acids [27, 28, 30], although the constant ($k = 2.22\ nm\ V^{-1}$) was little smaller than that of other electrolytes.

Figure 7 shows a) low and b) high magnification two-dimensional AFM images of an ideal cell arrangement fabricated by 3.0 M selenic acid anodizing at 46 V. Regular hexagonal dimples were formed on the aluminum substrate, and the bottom of each dimple was hemispherical in shape. Note that the sides of the hexagonal dimples were not flat and that characteristic convex parts that were approximately 20 nm in diameter formed at the triple points (indicated by the yellow arrows in Fig. 7b), where they were surrounded by three adjacent hexagonal dimples. These convex parts correspond to the most last anodizing point that is surrounded by the hexagonal alumina cells (shown in the schematic diagram insert in Fig. 7b). Three-dimensional AFM image of the ideal cell arrangement is shown in Fig. 8a, in which colors in the figure indicate the relative heights of the surface. Six convex parts (the dark blue and green regions, indicated by the yellow arrows) were located at the apexes of each hexagonal dimple (the violet and pink hemispherical regions). The height of the convex parts was approximately 40 nm, measured from the bottom of the hemispherical pores (Fig. 8b). These convex aluminum nanostructures with hexagonal arrangements may be useful as nanoelectrodes in various nanodevice applications, although further investigation of the electrodes will be required. Highly ordered nanosized electrodes may be able to be fabricated by selenic acid anodizing and selective oxide dissolution, as shown by the data in Figs. 7 and 8.

Figure 9 shows SEM images of a) the surface and b) the cross-section of the anodic porous alumina fabricated by the two-step selenic acid anodizing process. Two-step anodizing at an appropriate anodizing voltage enables the formation of highly ordered

anodic porous alumina without a nanoimprint technique because the nanopores are created at the bottom of the highly ordered hemispherical dimples formed by the first anodizing step (Fig. 8) [7]. For two-step anodizing, the aluminum foil was first anodized at 46 V for 180 min in a 3.0 M selenic acid solution, then the anodic oxide was selectively dissolved, and the aluminum foil was anodized again at 46 V for 3 min. After anodizing, the anodized specimen was immersed in an H_3PO_4 solution for 10 min to widen the pores. Highly-ordered anodic porous alumina that possessed a defect-free arrangement and has cell diameters of approximately 102 nm and pore diameters of approximately 40 nm was successfully fabricated by two-step anodizing in selenic acid. The porous alumina had parallel cylindrical nanoholes without an intercrossing structure and that had a high aspect ratio, as shown in Fig. 9b. Each wall of the anodic oxide was a slightly irregular straight line, which may be due to the mechanical cutting of the anodic porous alumina. The results of the selenic acid anodizing show its potential as an electrolyte for self-ordered anodic porous alumina fabrication much like the sulfuric, oxalic, and phosphoric acid electrolytes, previously reported. However, note that the cell size of the self-ordered porous alumina fabricated in selenic acid is different than the cell size that results from using other self-ordering electrolytes, as described bellow.

The self-ordering voltages of anodic porous alumina in various anodizing electrolytes and the corresponding oxide colors are summarized in Table 1. In addition to the voltage that resulted in the highly ordered alumina obtained by selenic acid anodizing in our present and previous investigations (V = 42, 46, and 48 V [55]), typical self-ordering voltages obtained in sulfuric (V = 19-25 V), oxalic (V = 40 V), malonic (V = 120 V), tartaric (V = 195 V), and phosphoric (V = 160-195 V) acid solutions are presented in Table 1 [28, 30]. Anodizing in selenic acid or oxalic acid causes the fabrication of ordered nanostructures at the voltage range of approximately 40 V, as shown in Table 1. However, note that the anodic oxide formed by selenic acid is colorless and transparent, whereas the oxide formed by oxalic acid has a yellowish color (Fig. 3). In addition, the saturated solubility of selenic acid in water is lager than that of oxalic acid. Therefore, selenic acid allows high speed anodizing at a high current density condition. Moreover, selenic acid anodizing can be used for fundamental research of anodizing science and engineering. A difference of the growth behaviors during anodizing in similar electrolyte solutions, selenic and sulfuric acid, should be investigated to understand the mechanism of porous alumina growth.

In summary, we demonstrated that highly ordered anodic porous alumina with a cell size different from that formed by anodizing in other electrolytes can be successfully fabricated by anodizing in selenic acid solution at appreciate electrochemical conditions. The ordered porous alumina can be fabricated by anodizing using a simple electrochemical setup and without using any special procedures such as the nanoimprint technique. Increasing the solution concentration is an effective method to achieve self-ordering with selenic acid anodizing. The regularity of the porous alumina obtained

by selenic acid anodizing is similar to the regularity obtained by anodizing with sulfuric, oxalic, or phosphoric acid. However, selenic acid anodizing works effectively at previously unutilized self-ordering voltages (V = 42-48 V) and the corresponding cell sizes (D = 95-110 nm). Therefore, selenic acid anodizing provides novel nanostructures in the field of highly ordered nanostructure applications. The self-ordered anodic porous alumina fabricated by selenic acid anodizing may be useful in various nanodevice applications including photonic crystals, plasmonic devices, magnetic recording media, and nanosensors. In addition, the convex aluminum nanostructures obtained by selenic acid anodizing and selective oxide dissolution may be useful as highly ordered nanoelectrodes in various nano-electronic devices.

4. Conclusions

This paper described the self-ordering behavior of anodic porous alumina fabricated using selenic acid anodizing at constant applied voltages and at various selenic acid concentrations. Anodizing in concentrated selenic acid solution causes rapid fabrication of anodic porous alumina with a highly regular cell arrangement. The self-ordered anodic porous alumina formed by selenic acid anodizing under the most appropriate electrochemical conditions, a concentration of 3.0 M and an anodizing voltage of 46 V, possesses a nanoporous structure with a cell size of 102 nm. Highly ordered convex nanostructures with diameters of approximately 20 nm and heights of approximately 40 nm were fabricated at the triple points by selenic acid anodizing and subsequent selective oxide dissolution and were surrounded by three adjacent hexagonal cells. Anodic porous alumina that is highly ordered from top to bottom can be successfully fabricated by two-step selenic acid anodizing.

Acknowledgements

The authors would like to thank Mr. Nobuyuki Miyazaki and Mr. Takashi Endo (Hokkaido University) for their assistance with SEM observations. This research was conducted at Hokkaido University and was supported by the “Nanotechnology Platform” Program of the Ministry of Education, Culture, Sports, Science and Technology (MEXT), Japan. This work was financially supported by the Japan Society for the Promotion of Science (JSPS) “KAKENHI”, the Japan Aluminium Association, and Toyota Physical & Chemical Research Institute Scholars.

References

1) R.C. Furneaux, G.E. Thompson, G.C. Wood, The application of ultramicrotomy to the electronoptical examination of surface films on aluminium, Corrosion Science 18 (1978) 853.
2) H. Habazaki, M.A. Paez, K. Shimizu, P. Skeldon, G.E. Thompson, G.C. Wood, The importance of surface treatment to the anodic oxidation behaviour of Al-Cu alloys, Corrosion Science 38 (1996) 1033.

3) T. Kikuchi, Y. Hara, M. Sakairi, T. Yonezawa, A. Yamauchi, H. Takahashi, Corrosion of Al–Sn–Bi alloys in alcohols at high temperatures. Part II: Effect of anodizing on corrosion, Corrosion Science 52 (2010) 2525.
4) Z. Ashitaka, G.E. Thompson, P. Skeldon, G.C. Wood, K. Shimizu, The Behavior of Copper and Lead during Heat‐Treatment and Surface Treatment of Aluminium Capacitor Foils, Journal of the Electrochemical Society 146 (1999) 1380.
5) K. Watanabe, M. Sakairi, H. Takahashi, S. Hirai, S. Yamaguchi, Formation of Al–Zr composite oxide films on aluminum by sol–gel coating and anodizing, Journal of Electroanalytical Chemistry 473 (1999) 250.
6) H. Uchi, T. Kanno, R.S. Alwitt, Structural features of crystalline anodic alumina films, Journal of the Electrochemical Society 148 (2001) B17.
7) H. Masuda, K. Fukuda, Ordered Metal Nanohole Arrays Made by a Two-step Replication of Honeycomb Structures of Anodic Alumina, Science 268 (1995) 1466.
8) T. Kikuchi, Y. Wachi, T. Takahashi, M. Sakairi, R.O. Suzuki, Fabrication of a meniscus microlens array made of anodic alumina by laser irradiation and electrochemical techniques, Electrochimica Acta 94 (2013) 269.
9) T. Kikuchi, Y. Wachi, M. Sakairi, R.O. Suzuki, Aluminum Bulk Micromachining through an Anodic Oxide Mask by Electrochemical Etching in an Acetic Acid / Perchloric Acid Solution, Microelectronic Engineering 111 (2013) 14.
10) H. Asoh, M. Matsuo, M. Yoshihama, S. ono, Transfer of nanoporous pattern of anodic porous alumina into Si substrate, Applied Physics Letters 83 (2003) 4408.
11) G. Macias, L.P. Hernandes-Eguia, J. Ferre-Borrull, J. Pallares, L. F. Marsal, Gold-coated ordered nanoporous anodic alumina bilayers for future label-free interferometric biosensors, ACS Applied Materials & Interfaces 5 (2013) 8093.
12) K. Yasui, T. Morikawa, K. Nishio, H. Masuda, Patterned magnetic recording media using anodic porous alumina with single domain hole configurations of 63 nm hole interval, Japanese Journal of Applied Physics 44 (2005) L469.
13) J. Choi, Y. Luo, R.B. Wehrspohn, R. Hillebrand, J. Schilling, U. Göele, Perfect two-dimensional porous alumina photonic crystals with duplex oxide layers, Journal of Applied Physics 94 (2003) 4757.
14) H. Jha, T. Kikuchi, M. Sakairi, H. Takahashi, Microfabrication of an Anodic Oxide Film by Anodizing Laser-textured Aluminum, Journal of Micromechanics and Microengineering 17 (2007) 1949.
15) S. Shukla, K-T. Kim, A. Baev, Y.K. Yoon, N.M. Litchinitser, P.N. Prasad, Fabrication and Characterization of Gold-Polymer Nanocomposite Plasmonic Nanoarrays in a Porous Alumina Template, ACS Nano 4 (2010) 2249.
16) J. Wang, M. Singh, M. Tian, N. Kumar, B. Liu, C. Shi, J.K. Jain, N. Samarth, T.E. Mallouk, M.H.W. Chan, Interplay between superconductivity and ferromagnetism in crystalline nanowires, Nature Physics, 6 (2010) 389.
17) H. Asoh, K. Nishio, M. Nakao, T. Tamamura, H. Masuda, Conditions for fabrication of ideally ordered anodic porous alumina using pretextured Al, Journal of

the Electrochemical Society 148 (2001) B152.
18) Y. Yamauchi, T. Nagaura, A. Ishikawa, T. Chikyow, S. Inoue, Evolution of standing mesochannels on porous anodic alumina substrates with designed conical holes, Journal of the American Chemical Society 130 (2008) 10165.
19) J.M. Giussi, I. Blaszczyk-Lezak, M.S. Cortizo, C. Mijangos, In-situ polymerization of styrene in AAO nanocavities, Polymer 54 (2013) 6886.
20) S. Samanman, C. Thammakhet, P. Kanatharana, C. Buranachai, P. Thavarungkul, Novel template-assisted fabrication of porous gold nanowire arrays using a conductive-layer-free anodic alumina oxide membrane, Electrochimica Acta 102 (2013) 342.
21) E. Kurowska, A. Brzózka, M. Jarosz, G.D. Sulka, M. Jaskuła, Silver nanowire array sensor for sensitive and rapid detection of H_2O_2, Electrochimica Acta 104 (2013) 439.
22) F. Keller, M.S. Hunter, D.L. Robinson, Structural Features of Oxide Coatings on Aluminum, Journal of the Electrochemical Society 100 (1953) 411.
23) G.E. Thompson, R.C. Furneaux, G.C. Wood, J.A. Richardson, J.S. Gode, Nucleation and growth of porous anodic films on aluminium, Nature 272 (1978) 433.
24) G.E. Thompson, G.C. Wood, Porous anodic film formation on aluminum, Nature 290 (1981) 230.
25) R.C. Furneaux, W.C. Rigby, A.P. Davidson, The formation of controlled-porosity membranes from anodically oxidized aluminum, Nature 337 (1989) 147.
26) G.E. Thompson, Porous anodic alumina: fabrication, characterization and applications, Thin Solid Films 297 (1997) 192.
27) S.Z. Chu, K. Wada, S. Inoue, M. Isogai, Y. Katsuta, A. Yasumori, Large-scale fabrication of ordered nanoporous alumina films with arbitrary pore intervals by critical-potential anodization, Journal of the Electrochemical Society 153 (2006) B384.
28) S. Ono, M. Saito, H. Asoh, Self-ordering of anodic porous alumina formed in organic acid electrolytes, Electrochimica Acta, 51 (2005) 827.
29) S. Ono, M. Saito, M. Ishiguro, H. Asoh, Controllong factor of self-ordering of anodic porous alumina, Journal of the Electrochemical Society 151 (2004) B473.
30) W. Lee, R. Ji, U. Gösele, K. Nielsch, Fast fabrication of long-range ordered porous alumina membranes by hard anodization, Nature Materials 5 (2006) 741.
31) H. Masuda, K. Takenaka, T. Ishii, K. Nishio, Long-range-ordered anodic porous alumina with less-than-30 nm hole interval, Japanese Journal of Applied Physics 45 (2006) L1165.
32) P. Chowdhury, A.N. Thomas, M. Sharma, H.C. Barshilia, An approach for in situ measurement of anode temperature during the growth of self-ordered nanoporous anodic alumina thin films: Influence of Joule heating on pore microstructure, Electrochimica Acta 115 (2014) 657.
33) H. Masuda, K. Yada, A. Osaka, Self-ordering of cell configuration of anodic porous

alumina with large-size pores in phosphoric acid solution, Japanese Journal of Applied Physics 37 (1998) L1340.
34) A-P. Li, F. Müller, A. Birner, K. Nielsh, U. Gösele, Polycrystalline nanopore arrays with hexagonal ordering on aluminum, Journal of Vacuum Science & Technology A 17 (1999) 1428.
35) M.A. Kashi, A. Ramazani, M. Noormohammadi, M. Zarei, P. Marashi, Optimum self-ordered nanopore arrays with 130–270 nm interpore distances formed by hard anodization in sulfuric/oxalic acid mixtures, Journal of Physics D: Applied Physics 40 (2007) 7032.
36) M.A. Kashi, A. Ramazani, M. Rahmandoust, M. Noormohammadi, The effect of pH and composition of sulfuric–oxalic acid mixture on the self-ordering configuration of high porosity alumina nanohole arrays, Journal of Physics D: Applied Physics 40 (2007) 4625.
37) S.J. Garcia-Vergara, P. Skeldon, G.E. Thompson, H. Habazaki, Tracer studies of anodic films formed on aluminium in malonic and oxalic acids, Applied Surface Science 254 (2007) 1534.
38) W. Lee, K. Nielsch, U. Gösele, Self-ordering behavior of nanoporous anodic aluminum oxide (AAO) in malonic acid anodization, Nanotechnology 18 (2007) 475713.
39) I. Vrublevsky, A. Jagminas, S. Hemeltjen, W. Goedel, Behavior of acid species during heat treatment and re-anodizing of porous alumina films formed in malonic acid, Journal of Solid State Electrochemistry 13 (2009) 1873.
40) V.F. Surganov, G.G. Gorokh, Anodic oxide cellular structure formation on aluminum films in tartaric acid electrolyte, Materials Letters 17 (1993) 121.
41) S. Ono, S. Chiaki, T. Sato, Micro-Structure of Anodic Oxide Film on Aluminum formed in Chromic Acid Solution, Journal of the Surface Finishing Society of Japan, 26 (1975) 456.
42) S. Ono, N. Masuko, Evaluation of pore diameter of anodic porous films formed on aluminum, Surface and Coatings Technology 169 (2003) 139.
43) W.J. Stępniowski, M. Norek, M. Michalska-Domańska, A. Bombalska, A. Nowak-Stępniowska, M. Kwaśny, Z. Bojar, Fabrication of anodic aluminum oxide with incorporated chromate ions, Applied Surface Science 259 (2012) 259.
44) T. Fukushima, Y. Fukuda, G. Ito, Y. Sato, Anodic Oxidation and Local Corrosion of Aluminum in Mono-carboxylic Acids, Journal of the Surface Finishing Society of Japan, 21 (1970) 319.
45) T. Kikuchi, T. Yamamoto, and R.O. Suzuki, Growth Behavior of Anodic Porous Alumina Formed in Malic Acid Solution, Applied Surface Science, 284 (2013) 907.
46) T. Fukushima, Y. Fukuda, G. Ito, M. Miyoshi, Anodic Oxidation of Aluminum at High Current Density in the Aqueous Solution of Hydroxycarboxylic Acids, Journal of the Surface Finishing Society of Japan, 25 (1974) 537.
47) A. Mozalev, I. Mozalev, M. Sakairi, H. Takahashi, Anodic film growth on Al layers

and Ta-Al metal bilayer in citric acid electrolytes, Electrochimica Acta, 50 (2005) 5065.
48) Y. Katsuta, A. Yasumori, K. Wada, K. Kurashima, S. Suehara, S. Inoue, Three-dimensionally nanostructured alumina film on glass substrate: Anodization of glass surface, Journal of Non-Crystalline Solids 354 (2008) 451.
49) T. Kikuchi, T. Yamamoto, S. Natsui, R.O. Suzuki, Fabrication of Anodic Porous Alumina by Squaric Acid Anodizing, Electrochimica Acta 123 (2014) 14.
50) M. Pashchanka, J. Schneider, Experimental validation of the novel theory explaining self-organization in porous anodic alumina films, Physical Chemistry Chemical Physics 15 (2013) 7070.
51) T. Kikuchi, O. Nishinaga, S. Natsui, R.O. Suzuki, Fabrication of Anodic Porous Alumina via Acetylenedicarboxylic Acid Anodizing, ECS Electrochemistry Letters 3 (2014) C25.
52) H. Takahashi, M. Nagayama, Electrochemical behavior and structure of anodic oxide films formed on aluminum in a neutral borate solution, Electrochimica Acta 23 (1978) 279.
53) A. Baron-Wiecheć, P. Skeldon, J.J. Ganem, I.C. Vickridge, G.E. Thompson, Porous Anodic Alumina Growth in Borax Electrolyte, Journal of the Electrochemical Society 159 (2012) C583.
54) H. Noguchi, A. Sano, Bath Temperature and Voltage Influence on Anodized Films on Aluminum in Organic Alkaline Baths, Journal of the Surface Finishing Society of Japan, 49 (1998) 649.
55) O. Nishinaga, T. Kikuchi, S. Natsui, R.O. Suzuki, Rapid fabrication of self-ordered porous alumina with 10-/sub-10-nm-scale nanostructures by selenic acid anodizing, Scientific reports 3 (2013) 2748.
56) T. Aerts, I. De Graeve, H. Terryn, Study of initiation and development of local burning phenomena during anodizing of aluminium under controlled convection, Electrochimica Acta 54 (2008) 270.
57) T. Aerts, I. De Graeve, H. Terryn, Anodizing of aluminium under applied electrode temperature: Process evaluation and elimination of burning at high current densities, Surface and Coatings Technology 204 (2010) 2754.
58) B. Gastón-García, E. García-Lecina, J. Díez, M. Belenguer, C. Müller, Local Burning Phenomena in Sulfuric Acid Anodizing: Analysis of Porous Anodic Alumina Layers on AA1050, Electrochemical Solid-State Letters 13 (2010) C33.
59) J.J. Roa, B. Gastón-García, E. García-Lecina, C. Müller, Mechanical properties at nanometric scale of alumina layers formed in sulphuric acid anodizing under burning conditions, Ceramics International 38 (2012) 1627.
60) H. Takahashi, Structure and Properties of Anodic Oxide Films on Aluminum and Their Micro- and Nano-Technology Application, in: T. Akiyama, et al. (Eds.), Frontiers of Materials Science, Ch. 2, Ohmsha, Tokyo, 2006, p. 26.
61) N. Baba, Functional Anodizing of Aluminum, Journal of the Aluminum finishing

Society of Kinki 94 (1982) 1.

Captions

Fig. 1 Schematic representation of the experimental apparatus for the selenic acid anodizing. The solution was stirred vigorously during anodizing.

Fig. 2 Change in current density, i, with anodizing time, t_a, in a a) 0.1 M, b) 1.0 M, and c) 3.0 M H_2SeO_4 solutions for 180 min at 273 K and constant cell voltages in the range of V = 37-51 V. Electropolished aluminum foils were anodized in the H_2SeO_4 solutions, and each solution was vigorously stirred by a magnetic stirrer during anodizing.

Fig. 3 Surface appearances of specimens anodized a) at 37 V in a 3.0 M H_2SeO_4 solution and b) at 40 V in a 0.22 M $(COOH)_2$ solution. After anodizing, the specimen was immersed in 0.5 M $SnCl_4$ solution to dissolve selectively the aluminum substrate.

Fig. 4 SEM images of the surface of the specimen anodized a) at 46 V in a 3.0 M H_2SeO_4 solution (uniform oxide formation) and b) at 51 V in a 0.1 M H_2SeO_4 solution (burning).

Fig. 5 Surface images of the anodized specimens after selective oxide removal by a 0.20 M CrO_3 / 0.51 M H_3PO_4 solution. The aluminum specimens were anodized in 0.1-3.0 M H_2SeO_4 solutions at various constant voltages in the range of 37 to 50 V for 180 min, as shown in Fig. 1.

Fig. 6 Effects of anodizing voltage, V, on the corresponding cell size, D, for 0.1-3.0 M selenic acid anodizing.

Fig. 7 a) Low and b) high magnification AFM images of the self-ordered nanodimple array. The specimen was anodized at 46 V for 180 min in a 3.0 M H_2SeO_4 solution.

Fig. 8 Three-dimensional AFM height images of the self-ordered nanodimple array at a) small and b) large angles.

Fig. 9 SEM images of the a) surface and b) cross section of the highly ordered anodic porous alumina fabricated with two-step anodizing. The second anodizing was carried out at 46 V for 3 min in 3.0 M H_2SeO_4 solution. The specimen was then immersed in a 0.86 M H_3PO_4 solution at 293 K to widen the pores.

Table 1 Electrolytes, self-ordering voltage, and the corresponding colors for anodic porous alumina formed in various acidic electrolytes (sulfuric, oxalic, malonic, tartaric, and phosphoric acids) reported previously [28, 30, 60, 61], as well as that of selenic acid found in the present and previous investigations [55].

Table 1

Electrolyte	Chemical formula	Color	Self-ordering voltage
Sulfuric acid	H_2SO_4	Transparent	19-25 V
Oxalic acid	$(COOH)_2$	Yellowish	40 V
Selenic acid	H_2SeO_4	Transparent	42-48 V
Malonic acid	$HOOC\text{-}CH_2\text{-}COOH$	Yellowish	120 V
Tartaric acid	$HOOC\text{-}(CHOH)_2\text{-}COOH$	Yellowish	195 V
Phosphoric acid	H_3PO_4	Light blue	160-195 V

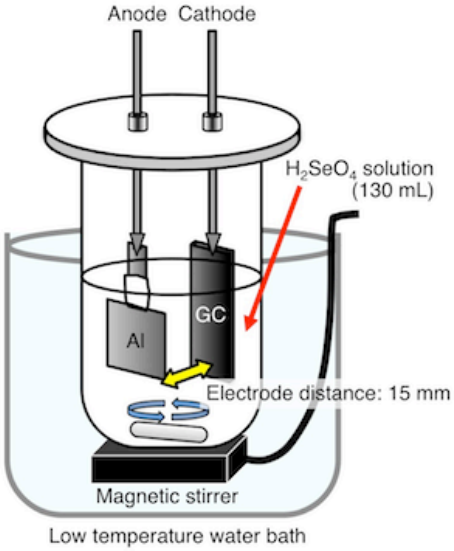
Anode Cathode
H_2SeO_4 solution
(130 mL)
GC
Al
Electrode distance: 15 mm
Magnetic stirrer
Low temperature water bath

Fig. 1

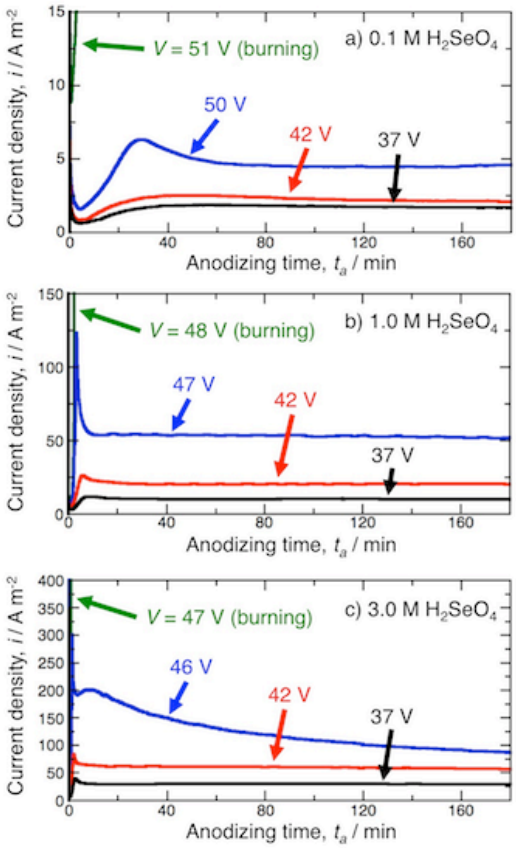
a) 0.1 M H_2SeO_4
V = 51 V (burning)
50 V
42 V
37 V
Current density, i / A m^{-2}
Anodizing time, t_a / min
b) 1.0 M H_2SeO_4
V = 48 V (burning)
47 V
42 V
37 V
Current density, i / A m^{-2}
Anodizing time, t_a / min
c) 3.0 M H_2SeO_4
V = 47 V (burning)
46 V
42 V
37 V
Current density, i / A m^{-2}
Anodizing time, t_a / min

Fig. 2

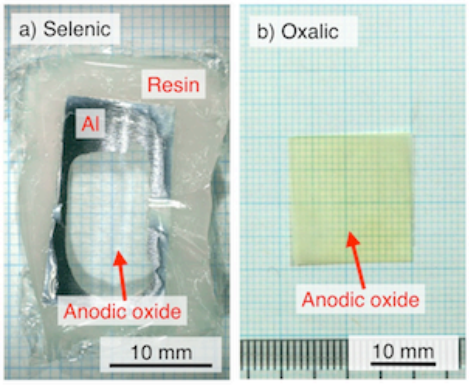
a) Selenic
Resin
Al
Anodic oxide
10 mm
b) Oxalic
Anodic oxide
10 mm

Fig. 3

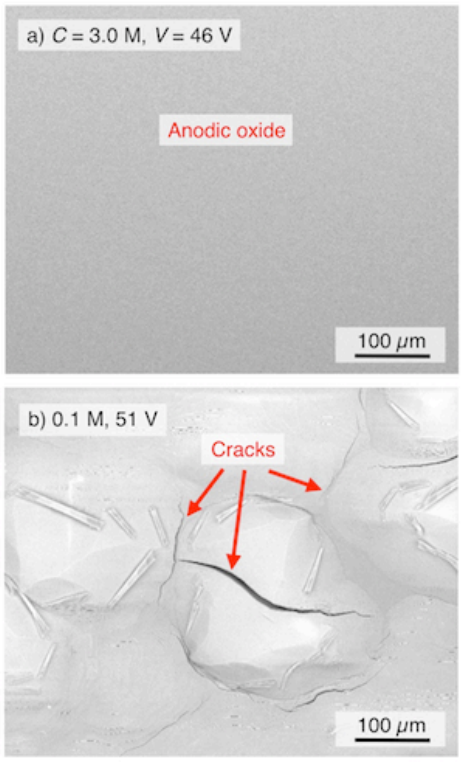

Fig. 4

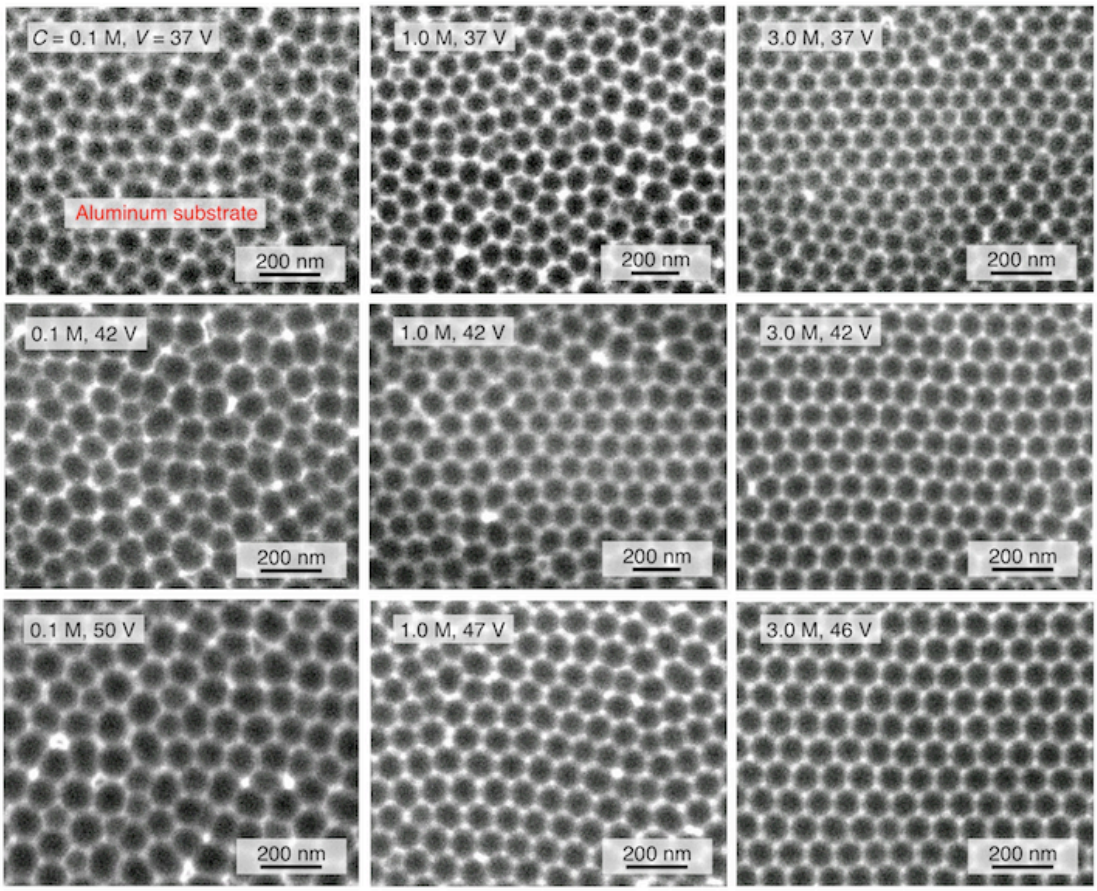
C = 0.1 M, V = 37 V
Aluminum substrate
200 nm
1.0 M, 37 V
200 nm
3.0 M, 37 V
200 nm
0.1 M, 42 V
200 nm
1.0 M, 42 V
200 nm
3.0 M, 42 V
200 nm
0.1 M, 50 V
200 nm
1.0 M, 47 V
200 nm
3.0 M, 46 V
200 nm

Fig. 5

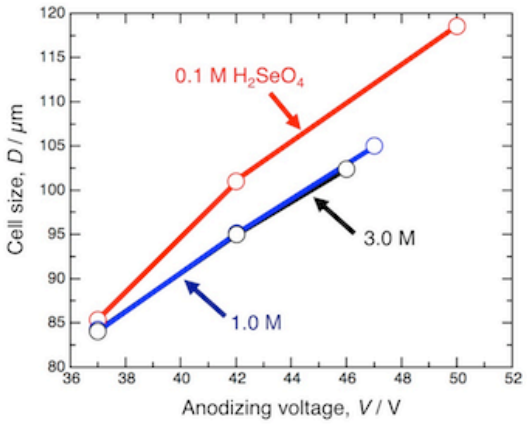
0.1 M H_2SeO_4
3.0 M
1.0 M
Cell size, D / μm
Anodizing voltage, V / V
120
115
110
105
100
95
90
85
80
36
38
40
42
44
46
48
50
52

Fig. 6

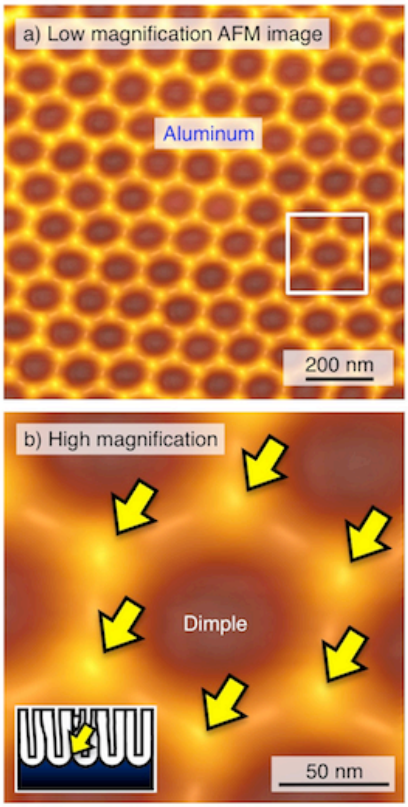
a) Low magnification AFM image
Aluminum
200 nm
b) High magnification
Dimple
50 nm

Fig. 7

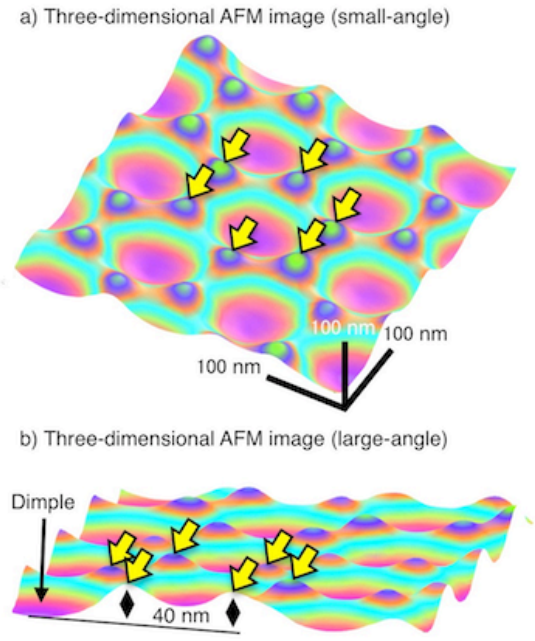
a) Three-dimensional AFM image (small-angle)
100 nm
100 nm
100 nm
b) Three-dimensional AFM image (large-angle)
Dimple
40 nm

Fig. 8

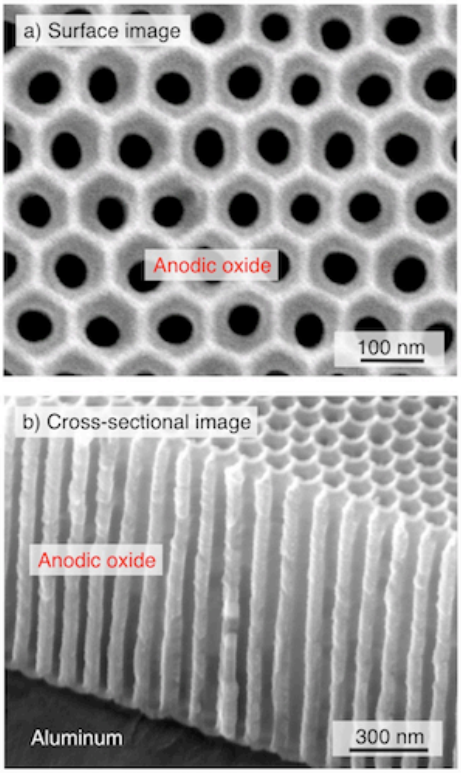
a) Surface image
Anodic oxide
100 nm
b) Cross-sectional image
Anodic oxide
Aluminum
300 nm

Fig. 9